Simple hybrid sea ice nudging method for improving control over partitioning of sea ice concentration and thickness

Alexandre Audette[1], **Paul J. Kushner**[1]

[1]Department of Physics, University of Toronto, 60 Saint George St., Toronto, ON, Canada, M5S 1A7

Key Points:

- Already established sea ice nudging method leads to issues in the partitioning between SIC and SIT.
- New hybrid nudging method significantly improves capture of both SIC and SIT targets for PAMIP, in particular for Arctic sea ice.
- Hybrid scheme increases Arctic turbulent heat flux and warming.

Corresponding author: Alexandre Audette, `alexandre.audette@utoronto.ca`

Abstract

To assess the effect of ocean-atmosphere coupling in the climate response to forced sea ice loss, the PAMIP (Polar Amplification Model Intercomparison Project) protocol includes centennial coupled atmosphere-ocean general circulation model simulations with imposed sea ice loss. The protocol, which specifies sea ice concentration and thickness distribution targets, does not prescribe a method for achieving them. Although different methods for imposing sea ice loss (or growth) in models have been documented, testing of the method-dependence of the resulting climate responses has been limited. Achieving the targeted sea ice state has proven to be challenging using the so-called *ghost-flux* nudging method, which induces ice melt from below, as this method does not constrain the partitioning between thickness and concentration. We propose, describe and test a simple method that combines the advantages of direct sea ice nudging and ghost-flux nudging. The hybrid nudging method better captures the partitioning between thickness and concentration while conserving total water content. We document how this novel sea ice constraining method reaches specific targets, enhances surface turbulent heat flux responses to sea ice loss, and induces tropospheric warming for both polar regions.

Plain Language Summary

The Arctic is warming faster than the global average due to several processes that, once combined, lead to so-called Arctic Amplification. Part of this anomalous polar warming comes from an intense reduction in ice cover allowing heat into the ocean, warming the Arctic ocean near the surface, and hence melting more ice. A joint effort by several climate modeling groups called the Polar Amplification Model Intercomparison Project (PAMIP) aims at better understanding Arctic Amplification through a coordinated set of climate simulations. Among this ensemble of simulations is a set of centennial simulations performed with fully coupled state-of-the-art climate models. In these experiments, Arctic (and Antarctic) sea ice are forced to reach specific states in order to better isolate Arctic Amplification and sea ice loss from the rest of anthropogenic global warming. In this paper, we propose a simple technique to nudge sea ice models to specific states such as prescribed by PAMIP. This new method combines advantages from existing techniques to improve the control over the extent and the thickness of the ice. We document in detail how our novel method leads to surface warming that previous work has shown is closely connected to sea ice loss from greenhouse warming.

1 Introduction

Over the past decades, observed Arctic sea ice extent (SIE) has greatly decreased, diminishing by nearly 50% in September (NSIDC, 2022). In the newer generation of climate models of the sixth phase of the Coupled Model Intercomparison Project (CMIP6, Eyring et al., 2016), the Arctic is projected to become seasonally sea-ice free before the year 2050 in all emissions scenarios (Notz & Community, 2020). In the opposite polar region, until the most recent five years, Antarctic SIE had been slowly increasing (Comiso et al., 2017), but the trend appears to now be reversing as the Antarctic witnesses reductions in SIE (NSIDC, 2022; Roach et al., 2020). Along with the reduction of sea ice cover, Arctic temperatures are rising more than twice as fast as the global average (Cohen et al., 2014). In Antarctica, a clear amplification of the warming is less clear, but this hiatus in air temperature trends might be coming to an end (Carrasco et al., 2021). This anomalous polar warming, referred to as Polar Amplification (PA), is caused by several local feedbacks and remote effects (Pithan & Mauritsen, 2014). In return, PA has important consequences on the whole climate system (Serreze & Francis, 2006).

The role that sea ice loss plays is central to understanding changes to the polar climate as well as the linkages between lower latitudes and the polar regions (Overland, 2016; Blackport et al., 2019). The Polar Amplification Intercomparison Project (PAMIP, D. M. Smith et al., 2019) attempts to elucidate the effects of PA from sea ice loss through a thoroughly specified experimental protocol that has so far been applied using several state-of-the-art Earth system models (e.g., Audette et al., 2021; Labe et al., 2020; D. M. Smith et al., 2022). Within this protocol are fully coupled climate simulations including atmosphere, ocean, ice and land model components. In particular, the *Group 6* experiments of PAMIP are extended centennial-scale coupled simulations in which specific Arctic and Antarctic sea ice states are targeted. Because of the technical limitations of different models, the method through which sea ice is constrained in the models is not prescribed by PAMIP, but different options are suggested in the protocol.

In order to constrain sea ice loss to specific targets, different techniques to achieve this have been developed over the years (e.g. Sun et al., 2018; K. L. Smith et al., 2014; Blackport & Kushner, 2016; Simon et al., 2021). The techniques in use generally fall into four categories: *albedo forcing* (Scinocca et al., 2009; Blackport & Kushner, 2016), *di-*

rect sea ice nudging (D. M. Smith et al., 2017), *ghost-flux forcing* (McCusker et al., 2017; Sun et al., 2018; Deser et al., 2015, 2016) and *ice-coupling forcing* (Dai et al., 2019).

- The albedo forcing method consists of modifying the albedo of sea ice and snow on sea ice to favor or restrain sea ice melt. Because the albedo value is fixed for the whole simulation, there is less control over the final equilibrium state of sea ice. This method amplifies the seasonal cycle, but naturally conserves energy and total water content.
- The direct sea ice nudging method consists of constraining sea ice to a specific target by measuring the difference between the simulated sea ice state and the target, then adding or removing a restoring amount of ice to the model. The algorithm usually adds or remove thickness and concentration independently. This method allows for precise control of the sea ice state but does not conserve energy or water. It is important to point out that nudging the ice could introduce spurious noise in the sea ice state as each time step as ice is added or removes.
- The ghost-flux nudging method consists of applying a restoring heat flux that melts the ice towards a certain state. This heat flux is only directly seen by the sea ice model and then by the other model components through sea ice changes. This method can be applied either interactively (Sun et al., 2018), similarly to the direct nudging method, or non-interactively (e.g. Deser et al., 2015), in which case it is usually referred to as *ghost-flux forcing*. This last approach does not control the sea ice state directly as it injects heat at the bottom of the ice and lets the melt and growth algorithms of the sea ice model deal with the changes in thickness and concentration of the ice. The ghost-flux nudging technique, however, conserves total water and salt content by construction, but does not conserve energy.
- The ice-coupling technique differs from the other methods above as it does not interact directly with the sea ice model. In this approach, the coupler and the atmosphere and ocean models only see a fixed sea ice target state while the sea ice model evolves freely. Because of this, some sea ice melt occurs near the ice edges, requiring the use of climatological surface fluxes over grid cells without ice. This step is necessary because the sea ice model in the Community Earth System Model, version 1 (CESM1, Hurrell et al., 2013) does not calculate these fluxes over grid cells without ice. The approach looks at the problem of sea ice loss from another perspective. Instead of studying the effect of sea ice loss on the climate system,

this technique allows the study of the effect of a fixed sea ice cover over on the climate including the ice itself through changes in the surface fluxes corresponding to this fixed state.

Although these methods have been used several times, very little direct comparison of them has been done. Because of this, it is still unclear how much the model's climate response depends on the method used to impose sea ice changes. Sun et al. (2020) compared ice albedo forcing to the ghost-flux nudging technique. Both methods showed very similar temperature and zonal mean responses, but the albedo forcing approach failed to capture the full extent of the polar winter response due to its underestimation of sea ice loss during that season. Screen et al. (2018) provides an overview of different sea ice loss simulations that use different models and different sea ice constraining methods. This comparison study notes some robust atmospheric circulation signals in all models, while noting some discrepancies in other fields, attributed to differences in the magnitude of sea ice loss and model background state. Inconsistencies like these complicate comparison of sea ice loss simulations from different sources, especially in regions like the subpolar North Atlantic, where the sea ice perturbation method can influence the oceanic response (e.g., Hay et al., 2022). We also note recent concerns that various sea-ice forcing methods might drive spurious Arctic amplification (England et al., 2021). The centennial coupled simulations of PAMIP aim at understanding the causes and consequences of PA through sea ice loss in a multi-model ensemble. Determining the robust aspects of the response, and addressing the realism of these experiments, first requires the development of a common and easily implemented method that allows for relatively precise consistency in the sea ice state.

The direct nudging method allows for precise control of the sea ice state, but can be difficult to implement because of the sea ice thickness (SIT) nudging part that can cause non-conservation issues in the advection step of the model. Modeling groups participating in PAMIP that are unable to constrain SIT are asked by PAMIP to only nudge sea ice concentration (SIC) directly and let SIT evolve freely. The ghost-flux nudging approach is more easily applicable in most climate models, but does not control the partitioning between SIC and SIT. In CICE4 (Hunke & Lipscomb, 2010), the sea ice model used in this study, the first effect of a bottom heat flux like the ghost-flux is a change

in the thickness of the ice, leading to eventual changes in concentration after the complete melt of the thinner parts of the sea ice in a grid cell.

Since the extended coupled PAMIP experiments have separate SIC and SIT targets, control over both variables is in principle required to reach the two targets. As described in more detail below, when we first attempted the PAMIP extended centennial coupled simulations, we used the ghost-flux nudging method by Sun et al. (2020). The results were, unfortunately, far from what we expected as the partitioning between SIC and SIT was not well captured. This motivated the development of the modified sea ice nudging method presented here. In this paper, we describe a novel, but still relatively simple, hybrid sea ice nudging method that combines part of the direct nudging method and the ghost-flux nudging method. The aim is to retain the water conservation property of ghost-flux nudging while increasing control over the extent of sea ice. This method is tested and compared to the ghost-flux nudging method using the PAMIP extended coupled simulations (pa-pdSIC-ext, pa-futArcSIC-ext & pa-futAntSIC-ext). Although we only show the results of this simple nudging method using one model (CESM1), we hope for this method to be applied to other models. In section 2, we describe the simulations used and compare the two methods. The results are discussed in section 3 and we finish with some concluding remarks and recommendations in section 4.

2 Methods

2.1 Model and simulations

We conduct the Group 6 experiments of PAMIP: pa-pdSIC-ext, pa-futArcSIC-ext and pa-futAntSIC-ext (D. M. Smith et al., 2019). These experiments are centennial coupled experiments integrated for at least 100 years each, in which both SIC and SIT are constrained to specific targets.

2.1.1 Fully coupled simulations

We conduct the sea ice loss perturbation experiments using CESM1. In particular, we use the Whole Atmosphere Community Climate Model, version 4, (WACCM4, Marsh et al., 2013) as the atmospheric component in its specified chemistry setting (SC-WACCM4, K. L. Smith et al., 2014). SC-WACCM4 is coupled to the Parallel Ocean Program, version 2 (POP2, R. Smith et al., 2010), to the Los Alamos sea ice model, version

4 (CICE4, Hunke & Lipscomb, 2010) and to the Community Land Model, version 4, (CLM4, Kluzek, 2012). The atmosphere and land models are at nominal 1.9° latitude by 2.5° longitude resolution and the sea ice and ocean models are run at a nominal resolution of 1° that becomes finer near the poles. A repeating 28-month cycle of the quasi-biennial oscillation obtained from observed radiosonde data is imposed in the atmospheric model through a nudging of the equatorial stratospheric winds (Peings et al., 2021).

The different methods used in this paper to constrain sea ice are implemented in CICE4. This sea ice model was originally created to be compatible with the ocean model POP and is an integral part of CESM1. In CICE4, the sea ice state is described through an ice thickness distribution (ITD). By default, five different thickness categories of fixed upper and lower thickness bounds are used in the ITD, in addition to open water. Sea ice melt and growth in this model happens through growth and melt at the bottom surface of the ice, top melt from surface heat absorption, and lateral growth and melt. This latter process is parametrized and mainly depends on the temperature difference between the ice and the ocean. Sea ice is then redistributed through the different categories to ensure each category remains within its bounds and the total concentration does not exceed 100%. Following melt and growth, a salt flux is added (or removed) to the ocean to compensate for the difference in salinity. As well, water is added or removed through water fluxes to the ocean when changes in sea ice volume occur.

In addition to the coupled experiments from PAMIP, we perform another fully coupled simulation that constrains sea ice to Year 2000 (Y2000) levels while doubling the CO_2 concentration compared to its Y2000 levels. The goal of this experiment is to characterize the ability of the hybrid nudging method to constrain sea ice in the presence of external and remote forcing.

2.1.2 CICE4 stand-alone simulations

In addition to the fully coupled simulations, we utilize a CICE4 "stand-alone" setup in the development of our hybrid nudging method. In this setup, the sea ice model is driven by a data atmosphere (DATM) and a data ocean (DOCN). These two components are non-interactive and are set to a Y2000 climatology (the default version of DATM and DOCN in CESM1). This implies that the atmospheric and oceanic forcings on sea ice will be constant in all simulations using this setup. These simulations were used in the

testing phase of our development of the hybrid nudging method because they are very inexpensive to run. As discussed later in section 2.3, the tuning in nudging using this stand-alone setup translate qualitatively to the fully coupled setup.

2.1.3 Atmosphere-land general circulation model (AGCM) simulations

For comparison purposes, we also utilize AGCM simulations performed using the same atmospheric model (SC-WACCM4) as the fully coupled simulations described in section 2.1.1. In these AGCM experiments, the sea surface temperature (SST) and sea ice boundary conditions are prescribed. These simulations have identical SIC and SIT targets as the fully coupled experiments, but prescribe a Y2000 climatological SST field described in D. M. Smith et al. (2019). The PAMIP protocol only calls for two of these experiments: pdSST-pdSICSIT and pdSST-futArcSICSIT, but for a comparison between the coupled ocean-atmosphere GCM and AGCM simulations we require a complementary experiment that imposes future SIC and SIT in the Antarctic, which we call pdSST-futAntSICSIT. The AGCM simulations consist of a 300-member ensemble for each experiment; each realization is integrated for 14 months, starting on April 1st (D. M. Smith et al., 2019). The first 2 months are discarded in the analysis to account for spin-up. The AGCM is in the same configuration as for the fully coupled simulations.

2.1.4 PAMIP sea ice targets

Each simulation is performed with specific SIC and SIT targets. In experiments with tags beginning pa-pdSIC-ext, Arctic and Antarctic sea ice fields are constrained to Y2000 sea ice. In experiments with tags beginning pa-futArcSIC-ext, Arctic sea ice is nudged to levels corresponding to a nominal +2°C global warming scenario from pre-industrial temperatures while Antarctic sea ice is held to Y2000 levels. In pa-futAntSIC-ext, Antarctic sea ice is nudged to +2°C global warming levels while Arctic sea ice is kept to Y2000 levels. Figures 4a-d-g-j and 5a-d-g-j show the targeted sea ice states for Y2000 and the difference between the future states and Y2000 in both polar regions. Sea ice in the model is constrained using two different methods: ghost-flux nudging as described in McCusker et al. (2017) and Sun et al. (2018) (experiments using this method are denoted with *-ghost*), and our proposed hybrid nudging method combining direct SIC nudging and ghost-flux nudging for SIT (experiments using this method are denoted with *-hyb*). A description of both methods and their implementation in CICE is given in sec-

Table 1. Summary table of the different simulations carried out for this study. The terminology is based on D. M. Smith et al. (2019).

Experiment name	Sea ice target	Nudging methodology
pa-pdSIC-ext-hyb	Y2000	Hybrid - Fully coupled
pa-futArcSIC-ext-hyb	Future Arctic, Y2000 Antarctic	Hybrid - Fully coupled
pa-futAntSIC-ext-hyb	Y2000 Arctic, Future Antarctic	Hybrid - Fully coupled
pa-pdSIC-2XCO2-ext-hyb	Y2000 (Double CO_2 concentration)	Hybrid - Fully coupled
pa-pdSIC-ext-ghost	Y2000	Ghost - Fully coupled
pa-futArcSIC-ext-ghost	Future Arctic, Y2000 Antarctic	Ghost - Fully coupled
pa-futAntSIC-ext-ghost	Y2000 Arctic, Future Antarctic	Ghost - Fully coupled
pa-pdSIC-cice-hyb	Y2000	Hybrid - CICE only
pa-futArcSIC-cice-hyb	Future Arctic, Y2000 Antarctic	Hybrid - CICE only
pa-futAntSIC-cice-hyb	Y2000 Arctic, Future Antarctic	Hybrid - CICE only
pa-pdSIC-cice-ghost	Y2000	Ghost - CICE only
pa-futArcSIC-cice-ghost	Future Arctic, Y2000 Antarctic	Ghost - CICE only
pa-futAntSIC-cice-ghost	Y2000 Arctic, Future Antarctic	Ghost - CICE only
pdSST-pdSICSIT	Y2000	Prescribed sea ice and SST
pdSST-futArcSICSIT	Future Arctic, Y2000 Antarctic	Prescribed sea ice and SST
pdSST-futAntSICSIT	Future Antarctic, Y2000 Arctic	Prescribed sea ice and SST

tion 2.2. We also perform the same simulations using the CICE4 stand-alone setup. A summary of the thirteen simulations is given in Table 1.

2.2 Nudging methods

2.2.1 Ghost-flux nudging

Ghost-flux nudging (McCusker et al., 2017; Sun et al., 2018) constrains the sea ice volume (SIV) at each model time step and grid cell in the sea ice model by applying a heat flux underneath the ice. The heat flux is proportional to the SIV difference between the target state and the model state, and is calculated according to

$$\delta F_{bot} = \frac{\rho_i L_i \left(h_i a_i - h_{target} a_{target}\right)}{\tau}, \tag{1}$$

where ρ_i is the density of sea ice, L_i is the latent heat of fusion of sea water, h_i is the simulated SIT, a_i is the simulated SIC, h_{target} is the target SIT, a_{target} is the target SIC and τ is the nudging timescale, set to 10 d as recommended in Sun et al. (2020). The heat flux δF_{bot} is added to the basal heat flux boundary condition in the basal melt calculation, and is thus only directly seen by the sea ice model, and indirectly felt by the rest of the model only through changes in sea ice. This nudging method automatically allows for conservation of salt content of the ocean and sea ice, while conserving total water content. This automatic conservation of salt and total water follows from the way sea ice melts with this technique. The heat flux applied on the lower ice boundary is added to the normal volume change calculation, which is then used in the salt and water conservation scheme. On the other hand, by nudging the product of concentration and thickness (volume), this method does not separately constrain concentration and thickness.

2.2.2 Hybrid nudging

We propose a simple hybrid between direct SIC nudging (D. M. Smith et al., 2017) and the ghost-flux nudging just described. In this method, both SIT and SIC are nudged independently to gain more control over the partitioning between concentration and thickness. This is important in order to capture the circulation and temperature response in the Arctic (Labe et al., 2020). First, the SIT is nudged using the ghost-flux method described previously, which allows for automatic conservation of the salt content and total water content coming from the thickness changes. The ghost-flux for the thickness nudging is given by

$$\delta F_{bot} = \frac{\rho_i L_i a_{target} \left(h_i - h_{target}\right)}{\tau_{sit}} \qquad \text{for all sea ice categories,} \tag{2}$$

where τ_{sit} is a nudging timescale set to 5 d in this study. We discuss the choice of timescale in section 2.3. The heat flux is also applied at the base of the sea ice.

In addition to the ghost-flux, we nudge SIC directly. To do this, we relax the SIC towards a target state by adding (or subtracting) a small quantity of sea ice area at every time step to the thinnest category of sea ice in the model. The restoring ice flux is

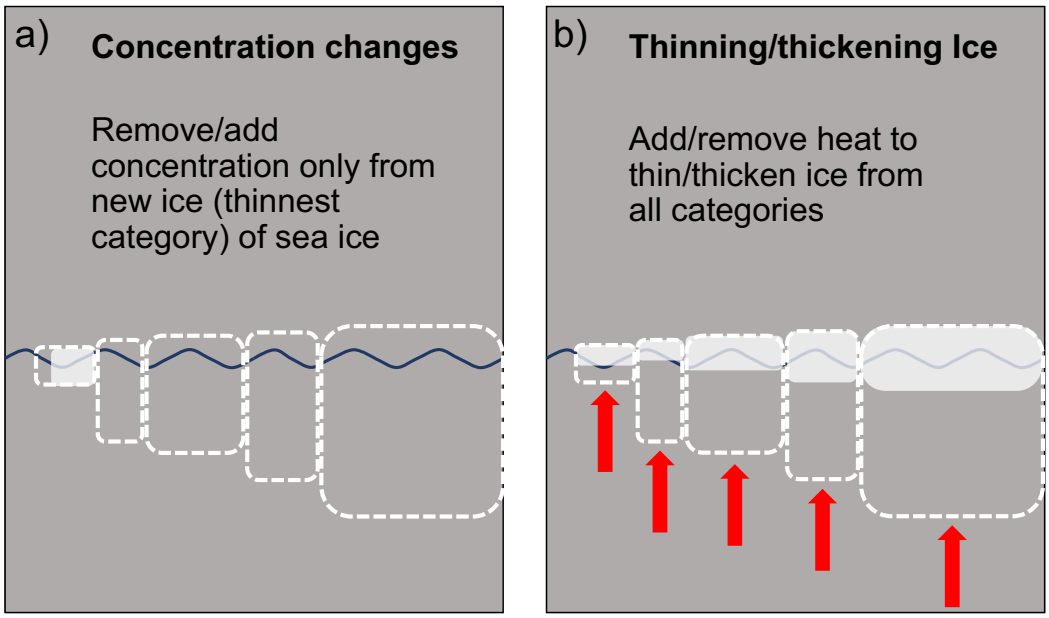

Figure 1. Schematic of nudging methodology for a) sea ice concentration nudging and b) sea ice thickness nudging via addition of a basal heat flux. Sea ice before nudging is represented by the white dash contour and sea ice after nudging is represented by the white shading. The red arrows represent the heat flux (measured in W/m^2) applied to the bottom of the ice.

calculated at every time step and is given by

$$\delta SIC = \frac{a_i - a_{target}}{\tau_{sic}} dt \qquad \text{for the thinnest ice category only,} \tag{3}$$

where τ_{sic} is the nudging timescale for the SIC nudging and dt is the time step of the sea ice model. τ_{sic} is set to 1 d, where again the choice of timescale will be discussed in section 2.3. At the end of the nudging step, the volume of snow on the ice is scaled to the new sea ice concentration meaning that the freshwater flux from snow melt due to nudging is neglected. This could be added into the algorithm in a future version.

As described above, CICE4 separates sea ice into five categories, from the thinnest to the thickest, allowing for a more realistic representation of SIT distribution at a smaller scale than the nominal resolution of the model. In order to avoid instabilities in the ice advection scheme and reduce non-conservation, we choose to add δSIC to the thinnest category of ice. This also avoids adding concentration to the thicker categories, which adds a relatively large amount of ice volume at once. A schematic representation of the hybrid nudging method is shown in Figure 1.

In addition to the ice flux, we add a freshwater flux (δf_{salt}) and the equivalent water mass (δf_{water}) from the ice melt coming from the direct sea ice concentration nudging. Both fluxes are calculated after the thickness change from the model melt and the nudging basal melt occur. The updated thickness h_{new} is multiplied by the change in concentration due to SIC nudging from equation (3) to get the change in volume from this part of the nudging. Both fluxes are described by

$$\delta f_{salt} = -\rho_i S_i h_{new} \delta SIC/dt \qquad \text{for the thinnest ice category only,} \tag{4}$$

$$\delta f_{water} = -\rho_i h_{new} \delta SIC/dt \qquad \text{for the thinnest ice category only,} \tag{5}$$

where S_i is the reference salinity of sea ice. These fluxes are added to the normal flux calculation when calculating the contribution of the thinnest ice category only.

2.3 Testing methods

Having discussed how the hybrid nudging method is defined, the final part of this section focuses on the methods we use to test this technique. To develop the hybrid nudging method, we first tested different variations of the ghost-flux nudging methods. These tests were performed using the CICE4 stand-alone setup described in section 2.1.2. This setup was chosen because it is inexpensive to run, and since after comparison with the fully coupled model, the improvements in that stand-alone setup qualitatively translated to the fully coupled version (see Figure S2 (S3) in comparison with Figure 4 (5)). The data-driven CICE4 provides a good and inexpensive test bench for sea ice nudging techniques. Overall, where the sea ice agreement with the target improved in the data-driven CICE4, the agreement also improved in the fully coupled set up. In fact, the improvement is better in the fully coupled simulations because the atmosphere and ocean can respond to the sea ice forcing, strengthening the effect of the nudging algorithm. This strengthening effect mostly comes through the ice albedo feedback which can act to increase sea ice melt when the nudging algorithm reduces the ice cover, or decrease sea ice melt when the nudging grows ice.

To determine good nudging timescales (τ_{sic} and τ_{sit}) we perform 10-year long fully coupled simulations with several combinations of nudging timescales for the pa-pdSIC-ext experiment. An integration of ten years was deemed to be enough as the sea ice usually equilibrated after two to three years with the nudging. We optimize the values of

the nudging timescales for the present day run. We range τ_{sit} over 1, 5, 10 and 50 d, and τ_{sic} over 0.1, 0.5, 1 and 5 d. With this range of timescales, we span about two orders of magnitude of timescales for both variables. We compare the root mean square error (RMSE) and the mean bias of all simulations for both Arctic and Antarctic SIC and SIT. Both the mean bias and RMSE are calculated over grid cells containing either sea water or sea ice northward of 66°N for Arctic sea ice and southward of 60°S for Antarctic sea ice.

To compare the performance of SIC and SIT nudging, we offset the RMSE and mean bias values by their respective minimum and scale by the range of values to put everything on a scale between 0 and 100 where a score of 0 is best and 100 is worst. We then average the score for both sea ice variables and rank the nudging timescale combinations from best (1) to worst (16) (see Figure 2).

Most of the changes in performance for Arctic sea ice come from changes in τ_{sit}, and the trends of changes in performance are opposite for SIC and SIT. For SIC, larger τ_{sit} values (weaker bottom nudging) lead to smaller mean bias and RMSE values (Figures 2a and 2d). This is likely due to an overall weaker constraint on sea ice from that part of the nudging, which allows for a better separate control by the SIC nudging. Inversely and non surprisingly, smaller τ_{sit} values lead to better performance for Arctic SIT nudging. Variations in τ_{sic} do not consistently affect the results in the northern polar region (Figure 2b and 2e).

The opposition between the direction of the improvement in nudging between SIT and SIC is less clear for the southern polar region (Figure S1). The overall tendency of the quality of Antarctic SIC still improves with larger values of τ_{sit}, but the stronger SIC nudging leads to improvement in SIC (Figure S1a and S1d). The quality of the Antarctic SIT nudging (Figure S1b and S1e) is very similar to the Arctic SIT nudging score, improving with smaller τ_{sit} values.

The timescale combinations are ranked from best (1) to worst (16) in Figure 2c and 2f (Figure S1c and S1f for Antarctic sea ice). Overall, the best performing timescale combination for Arctic sea ice nudging is 1 day for τ_{sic} and 5 days for τ_{sit} and is highlighted in red in these panels. This combination is not unsurpassed in any of the two metrics we use, but is the best when looking at both combined. For Antarctic sea ice nudging, the combination leading to the highest rank (0.5 day for τ_{sic} and 1 day for τ_{sit}) differs

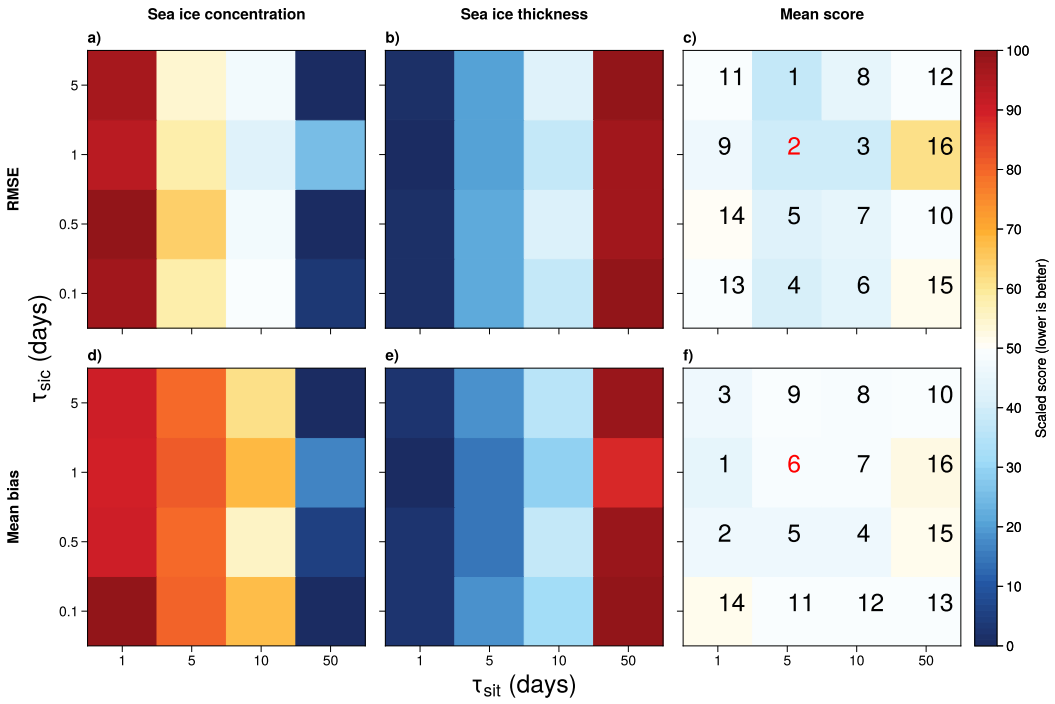

Figure 2. Root mean square error and mean bias scores of different nudging timescale combinations. a) RMSE score of Arctic SIC. b) As in a) but for Arctic SIT. c) Mean RMSE score of both Arctic SIC and SIT. In panel c), the numbers indicate the rank of each combination for the mean RMSE score. d)-f) As in a)-c) but for the mean bias. The numbers highlighted in red in panels c) and f) indicate the best overall score over both performance metrics.

from the Arctic nudging. However, when combining the scores for both poles, the best combination remains 1 day for τ_{sic} and 5 days for τ_{sit}.

3 Results

This section describes the improvements that hybrid nudging provides compared with ghost-flux nudging, based on achieving target Arctic and Antarctic sea ice states and sea ice loss responses, and on aspects of surface warming and atmospheric circulation responses from Arctic and Antarctic sea ice loss corresponding to +2°C of global warming.

3.1 Agreement with PAMIP target

Figure 3 shows the seasonal cycle of the effective thickness (or mean SIV), the mean SIT, and the total sea ice area in the Arctic and Antarctic. The effective thickness/mean SIV is defined as the average volume of sea ice in a grid cell per area of that grid cell poleward of 66° North (or of 60° South for Antarctic sea ice) in grid cells where there is either sea ice or open water. In comparison, the mean SIT is defined as the mean thickness of sea ice, not counting regions with open water. All averages are weighted by grid cell area. The climatological average is taken over the final 40 years of the simulations.

The mean SIV is shown in Figures 3a-b for both methods. The mean absolute difference between the two methods is minimal for all targets in both polar regions (less than 0.02 m^3/m^2 on average) for SIV. The mean and maximum differences are shown in Tables 2 and 3. When using the ghost-flux nudging technique, the effective SIT is well simulated. The hybrid nudging method maintains this characteristic of the ghost-flux nudging as the thickness is nudged similarly.

For mean SIT, the hybrid nudging method is able to capture the thicker sea ice in the Arctic better than the ghost-flux method during the boreal winter months in both present day and future states (Figure 3c). The hybrid nudging decreases the maximum magnitude of the bias by close to half in the Arctic for both targets and by about a third in the Antarctic for both targets (see Tables 2 and 3 for exact numbers), relative to the ghost-flux nudging. The boreal summer months do not show much differences in the Arctic in pa-futArcSIC-ext, but larger differences arise in pa-pdSIC-ext. Indeed, the hybrid nudging method better reaches the minimum in August, but does not capture the full extent of the local maximum in September through November, where the ghost-flux nudging method does better. Overall, the ghost-flux nudging method better captures the summer thickness in the Arctic than the hybrid nudging method, but the differences remain small (on the order of 10 cm). In the southern polar region, both methods show too thick ice during the Austral summer in both pa-pdSIC-ext and pa-futAntSIC-ext (Figure 3d). Overall, hybrid nudging brings the thickness down slightly in the Southern Ocean.

The total sea ice area seasonal cycle shows the largest difference between the two methods (Figures 3e and 3f). We show the total sea ice area agreement with the target. Overall, the hybrid nudging significantly improves sea ice area control in both hemisphere (reduces the mean absolute bias by about half). More specifically, Arctic sea ice area matches

Table 2. Mean absolute differences and differences of maximum magnitude for ghost-flux nudging, hybrid nudging and the PAMIP targets for the seasonal cycles of Arctic mean SIT, SIA and SIV in pa-pdSIC-ext and pa-futArcSIC-ext. The maximum difference (together with the sign of the difference) is shown in parentheses.

Arctic sea ice in pa-pdSIC-ext			
Comparison	Thickness (m)	Area (10^6 km^2)	Volume (m^3/m^2)
Ghost-flux minus Hybrid	0.05 (0.11)	0.51 (-1.1)	0.02 (-0.04)
Ghost-flux minus target	0.08 (0.21)	1.2 (-2.7)	0.04 (-0.14)
Hybrid minus target	0.08 (-0.15)	0.57 (-1.8)	0.04 (-0.10)
Arctic sea ice in pa-futArcSIC-ext			
Comparison	Thickness (m)	Area (10^6 km^2)	Volume (m^3/m^2)
Ghost-flux minus Hybrid	0.04 (-0.08)	0.53 (1.1)	0.00 (0.01)
Ghost-flux minus target	0.10 (-0.18)	1.1 (-2.4)	0.02 (0.04)
Hybrid minus target	0.06 (-0.16)	0.63 (-1.8)	0.02 (0.04)

very well with the target state when using hybrid nudging and this new method removes the January-April positive bias in pa-futArcSIC-ext and a good portion of the July-November negative bias in pa-pdSIC-ext exhibited by the ghost-flux nudging method. Although agreement with the Antarctic sea ice area remains imperfect, the strategy adopted here of concentration restoring on thin sea ice provides a net improvement. The low bias of the model in the Antarctic case during the months of July to November might be associated with the model climatology. In particular, the unforced (free-running) model's climatological sea ice area is less than that of the PAMIP target (not shown). The nudging is thus working against the tendency of the coupled simulation to produce this low sea-ice state, but is strong enough to push the sea ice state towards the PAMIP target. Since different models might have different sea ice climatologies; the results found here might change slightly with different models.

Figure 4 maps the annual mean Arctic SIC and thickness and their biases compared to the target state. Figure 4a shows the annual mean SIC target for pa-pdSIC-ext and Figure 4b displays the differences between the simulated climatological SIC using ghost-flux nudging and the target climatology. The corresponding map for hybrid nudging is

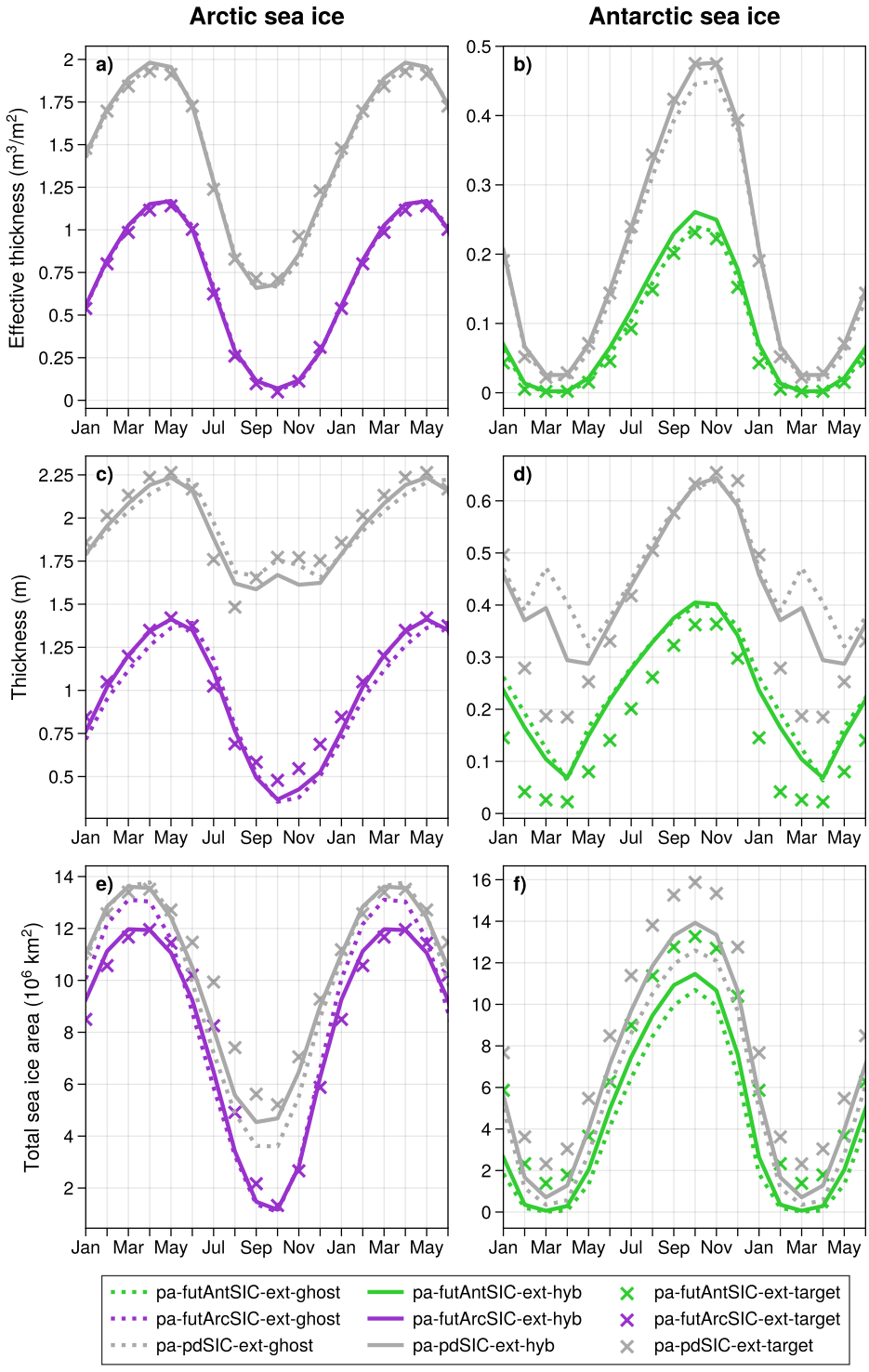

Figure 3. Seasonal cycle of the sea ice state for both the ghost-flux (dotted) nudging and hybrid nudging (solid) methods. a) Effective sea ice thickness (mean thickness over the Arctic) for pa-pdSIC-ext (grey), pa-futArcSIC-ext (magenta). b) As in a) but for Antarctic sea ice and pa-futArcSIC-ext (green). c) As in b) but for mean Arctic SIT north of 66°. d)-f) As in a)-c) but for Antarctic sea ice. The "×" represent the targets for each variable, in grey for the Y2000 target, magenta for the future Arctic target and green for the future Antarctic target.

Table 3. Mean absolute differences and maximum differences between ghost-flux nudging, hybrid nudging and the PAMIP targets for the seasonal cycles of Antarctic mean SIT, SIA and SIV in pa-pdSIC-ext and pa-futAntSIC-ext. The maximum difference is shown in parentheses.

	Antarctic sea ice in pa-pdSIC-ext		
Comparison	Thickness (m)	Area (10^6 km^2)	Volume (m^3/m^2)
Ghost-flux minus Hybrid	0.02 (0.11)	0.98 (-1.4)	0.01 (0.02)
Ghost-flux minus target	0.07 (0.28)	2.8 (-3.3)	0.01 (0.15)
Hybrid minus target	0.04 (0.20)	1.8 (-2.1)	0.00 (0.12)
	Antarctic sea ice in pa-futAntSIC-ext		
Comparison	Thickness (m)	Area (10^6 km^2)	Volume (m^3/m^2)
Ghost-flux minus Hybrid	0.01 (0.07)	0.69 (-1.0)	0.01 (-0.02)
Ghost-flux minus target	0.07 (0.15)	2.6 (-4.0)	0.00 (0.01)
Hybrid minus target	0.06 (0.12)	1.9 (-3.2)	0.01 (0.02)

shown in Figure 4c. The ghost-flux nudging technique leads to local biases up to 25% in the peripheral Arctic and exhibits an average negative bias of −3.7% over the Arctic. In comparison, hybrid nudgingshows local biases that reach about 15% and reduces the mean bias in SIC to −1.6% and RMSE from 7.8% to 5.3% compared to the ghost-flux nudging method. Figure 4d displays the target Arctic SIC melt between the pa-futArcSIC-ext and pa-pdSIC-ext experiments, representing the CMIP5 multimodel mean under 2°C of global warming (D. M. Smith et al., 2019). Most sea ice loss takes place in the Beaufort, Barents and Kara Seas. Figure 4e illustrates the difference between simulated SIC loss with the ghost-flux nudging method and the targeted SIC loss. When using the ghost-flux nudging method, not enough sea ice melts over most of the Arctic. This particular challenge in this method is imposing the intended SIC loss in the Barents and Kara Seas. This leads to a mean bias of 3.4% and RMSE of 6.3%. As for the Y2000 SIC simulation, the hybrid nudging method (Figure 4f) greatly reduces the mean bias to 0.65% and RMSE to 3.6%.

The equivalent maps for SIT are shown in Figures 4g-l. Overall, and as mentioned above for the seasonal cycle of SIT, both methods area able to constrain sea ice thickness in both pa-pdSIC-ext and pa-futArcSIC-ext. Both methods show similar RMSE and

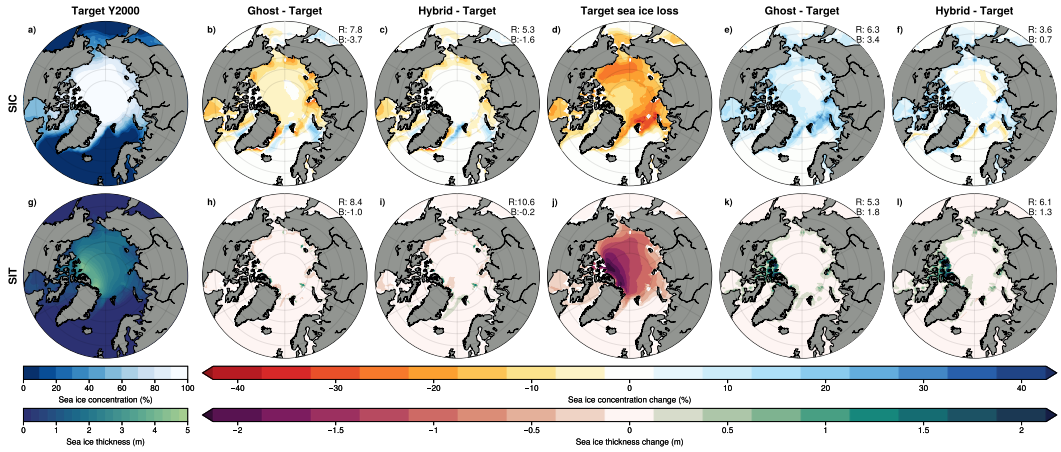

Figure 4. Annual mean Arctic SIC and thickness in the PAMIP simulations. a) SIC target in pa-pdSIC-ext. b) Difference between simulated SIC and target SIC in pa-pdSIC-ext-ghost. c) As in b) but for the pa-pdSIC-ext-hyb experiment. d) Target SIC changes between pa-futArcSIC-ext-hyb and pa-pdSIC-ext-hyb. e) Difference in simulated melt between pa-futArcSIC-ext-ghost and pa-pdSIC-ext-ghost. f) As in e) but for pa-futArcSIC-ext-hyb and pa-pdSIC-ext-hyb. g)-l) As in a)-f) but for SIT. The numbers on the top right corner of the panels in columns 2, 3, 5 and 6 indicate the area weighted root mean square error (R) and mean bias (B). For SIT (SIC), the RMSE and mean bias are displayed in units of cm (%).

mean bias for the Y2000 control state (Figures 4h-i), the hybrid nudging increases slighlty the RMSE by 1.8 cm, but reduces the mean bias by 0.8 cm. Similarly, the hybrid nudging method increases slightly the RMSE for the mean sea ice thickness (by 0.8 cm), but reduces the mean bias by 0.5 cm when it comes to the targeted melt (Figure 4k-l).

The annual mean Antarctic SIC and SIT are shown in Figure 5. Although both methods broadly underestimate SIC (Figure 3f), the hybrid nudging method shows significant improvements in the Antarctic SIC over the ghost-flux nudging. This new method is able to halve the mean bias that the ghost nudging produces in SIC nudging and reduces the RMSE by about a third (Figures 5b-c). Still, important SIC biases of about 20% remain in the Weddell Sea and the western part of the Ross Sea when using the hybrid nudging method. The improvement is also evident in Figures 5e-f. Indeed, the hybrid nudging method is able to reduce the RMSE from 1.0% to 0.3%, without any substantial improvement in the mean bias. Both methods display a common issue when it comes to reaching the SIC melt target: sea ice appears to be too widely spread out north-

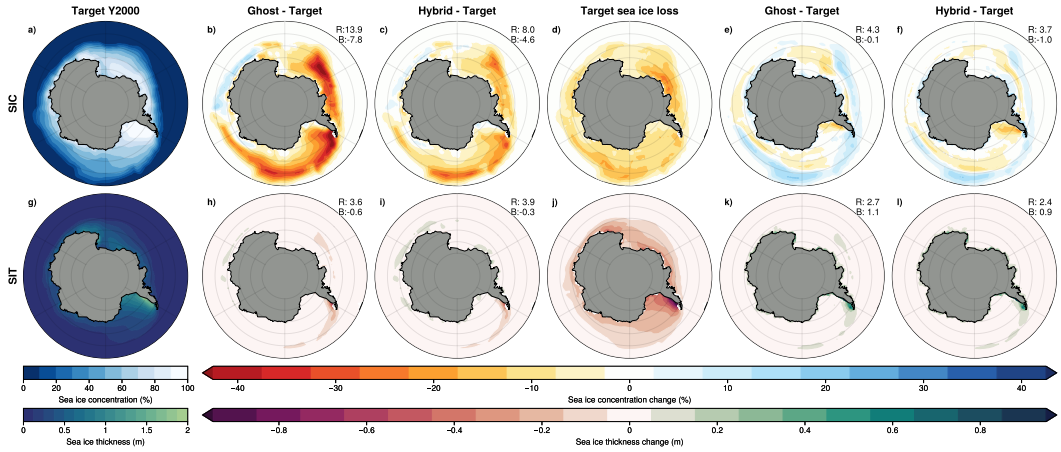

Figure 5. As in Figure 4 but for Antarctic sea ice using pa-futAntSIC-ext-hyb and pa-futAntSIC-ext-ghost instead of pa-futArcSIC-ext-hyb and pa-futArcSIC-ext-ghost

ward in most of the Southern Ocean. The ghost-flux nudging method shows this issue in a more pronounced way, but the hybrid nudging method has a stronger negative bias in the Weddell sea on the coast of the Antarctic Peninsula. In a similar fashion as for Arctic SIT, Antarctic SIT nudging sees little differences between the two methods for the Y2000 sea ice state (Figures 5h-i). Both methods show too thin ice near the tip of the Antarctic Peninsula and the SIT distribution changes very little. The RMSE increases by 1.8 cm with the hybrid nudging method, but this same method reduces the mean bias by 0.5 cm. The SIT melt using both methods is shown in Figures 5k-l. Both methods manage to constrain SIT melt within a RMSE of about 1 cm and both have a mean bias of less than 1 mm. Overall, the hybrid nudging improves significantly the constraining of SIC and only slightly improves SIT, although it creates a slightly larger error in SIC melt in the Weddell Sea.

3.2 Effect of nudging methods on Arctic and Antarctic climate

To assess aspects of the climate response to sea-ice forcing, we now compare the air temperature surface turbulent heat flux and circulation responses when using ghost-flux nudging, hybrid nudging and AGCM experiments, described in section 2.1.3, with the same prescribed SIC and SIT at the coupled experiments. For the AGCM experiments, we use the pdSST-pdSICSIT, pdSST-futArcSICSIT and pdSST-futAntSICSIT

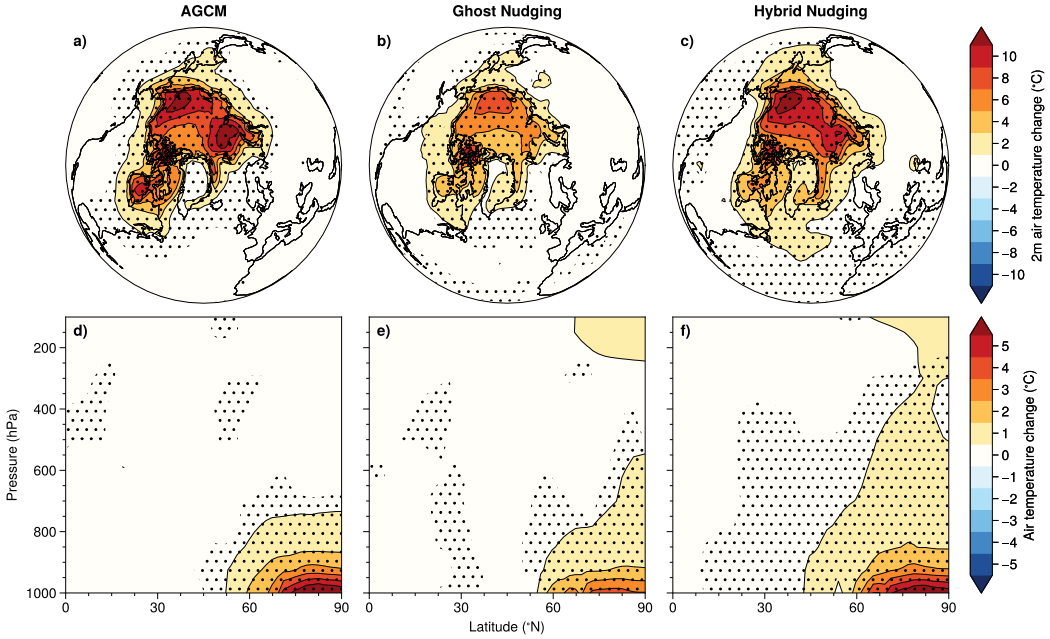

Figure 6. DJF air temperature change with different sea ice constraining methods. a) 2m Arctic air temperature change between pdSST-futArcSICSIT and pdSST-pdSICSIT (prescribed SST and SIC). b) As in a) but between the pa-futArcSIC-ext-ghost and pa-pdSIC-ext-ghost experiments (ghost-flux nudging). c) As in a) but between the pa-futArcSIC-ext-hyb and pa-pdSIC-ext-hyb experiments (hybrid nudging). d)-f) As in a)-c) but for the DJF zonal mean air temperature response. The statistical significance to a 95% confidence level with a Student t-test is indicated by the stippling.

simulations as described in section 2.1.3. For the coupled simulations, the final 40 y of simulations are averaged.

In Figure 6a, the 2m air temperature response to sea ice loss is shown for the AGCM simulation. In this case, the 2m air temperature response displays four localized maxima over the Hudson Bay, the Canadian Arctic Archipelago, the Beaufort Sea and the Barents and Kara seas. Each maximum matches very well with the prescribed SIC loss pattern shown in Figure 4d, except the warming spot in the Canadian Arctic which matches better with the SIT changes in Figure 4j, and apparently stems from thinning of SIT (Labe et al., 2020). In comparison, the 2m air temperature response in the coupled experiment using ghost-flux nudging (Figure 6b) only shows two clear maxima, one over the Beaufort Sea and the other over the Canadian Arctic Archipelago. The warming maxima lo-

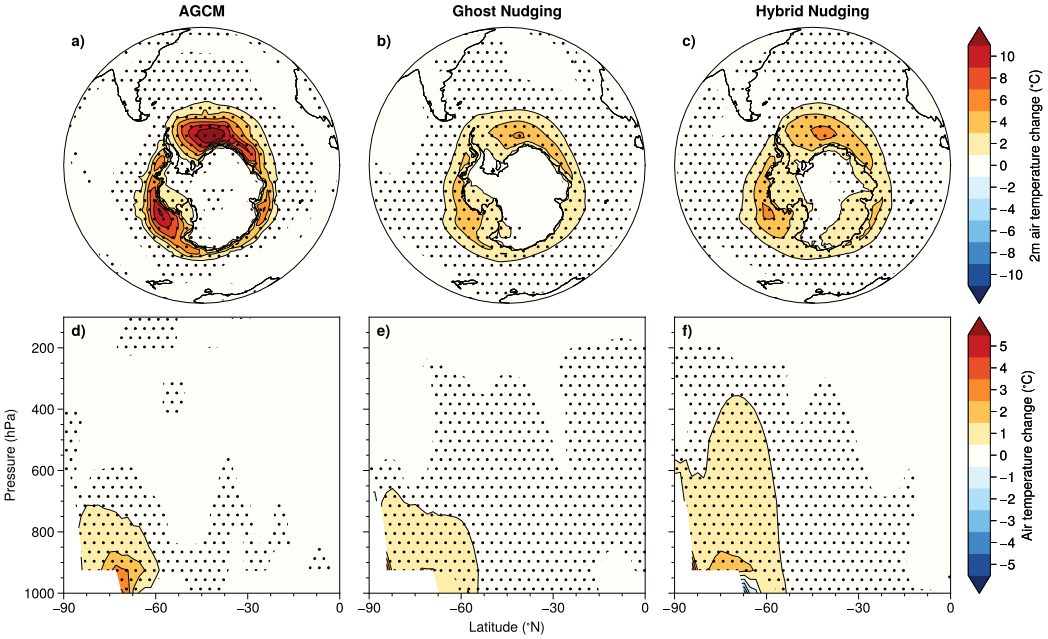

Figure 7. As in Figure 6, but for the JJA air temperature response to Antarctic sea ice loss in the Southern Hemisphere.

cated over the Barents and Kara Seas and Hudson Bay in Figure 6a are absent in Figure 6b. This lack of warming signals corresponds to the positive biases in SIC change over these regions in Figure 4e. The 2m air temperature response when using the hybrid nudging method (Figure 6c) is qualitatively akin to the AGCM response (Figure 6a). This nudging method recovers the Barents and Kara seas signal and warms more over Hudson Bay than than the ghost-flux nudging simulation. However, the warming signal over Hudson Bay remains less than the AGCM simulation. Overall, the warming signal with the hybrid nudging is also stronger than with the AGCM runs, similarly to what other studies have found (Deser et al., 2016).

Furthermore, the vertical structure of the temperature response, represented by zonal mean cross sections in Figure 6d-f, differs significantly when comparing the three set ups. First, the AGCM response (Figure 6d) is confined to the lower troposphere and extends equatorward of 50°N. The ghost-flux nudging response (Figure 6e) seems even more confined to the lower troposphere North of 60°N, and is weaker in intensity. Finally, the zonal mean temperature response with the hybrid nudging (Figure 6f) extends deeper into the mid-latitudes and higher into the Arctic troposphere and lower stratosphere.

For the corresponding thermal responses for Antarctic sea ice loss, the AGCM response is about 2-3 times stronger than the coupled model response with both methods (Figures 7a-c), which is consistent with previous Antarctic sea ice loss experiments (D. M. Smith et al., 2017, Figure 2). The surface warming from the hybrid nudging (Figure 7c) is stronger than from ghost-flux nudging (Figure 7b), although both have very similar spatial patterns. This is most likely due to the larger amount of sea ice loss in the hybrid nudging simulations. Similarly to the Arctic warming warming signal, the vertical extent of the warming is larger with the hybrid nudging (7f), the warming signal extending up to 400 hPa compared to 700 hPa for the AGCM response (7d) and 550 hPa for the ghost-flux nudging experiment (7e).

In Figure 8, the surface sensible and latent heat fluxes are shown along with the near-surface air temperature for the AGCM and coupled simulations. The climatologies (grey lines), responses to Arctic sea ice loss (magenta lines) and responses to Antarctic sea ice loss (green lines) are shown on the same plots. In the zonal and annual mean, we note that the climatological sensible heat flux, latent heat flux, and 2m air temperature are similar in the AGCM and coupled control simulations (grey lines in Figures 8a-d-g). This is consistent with our general observation that the climatological present-day control state is similar in the PAMIP AGCM and coupled simulations (not shown), providing a controlled background state for subsequent perturbations in the two types of simulations. In response to Arctic sea ice loss (magenta lines), both nudging methods lead to an increase in sensible heat heat flux. However, the increase north of 60°N is about twice as large (up to 4 W/m^2) when using the hybrid nudging method compared to the ghost-flux nudging method. The hybrid nudging method also matches very well the AGCM response in the Arctic. The imbalance created in the climatological sensible heat flux is of similar intensity for the hybrid nudging method and the AGCM simulations, with the ghost-flux nudging leading to an apparent underestimation of the response. This follows from a larger change in sea ice cover when using this method since more ocean surface is exposed to the atmosphere.

The Arctic seasonal cycle in Figure 8b also demonstrates this consistency between the AGCM and the coupled hybrid-nudging simulations with a larger response in sensible heat flux in the winter season, where most of the improvement in SIC is seen in Figure 3e. The difference between the two methods is less clear in response to Antarctic sea ice loss (green lines) in Figure 8a. Actually, both methods show an increase in sensible

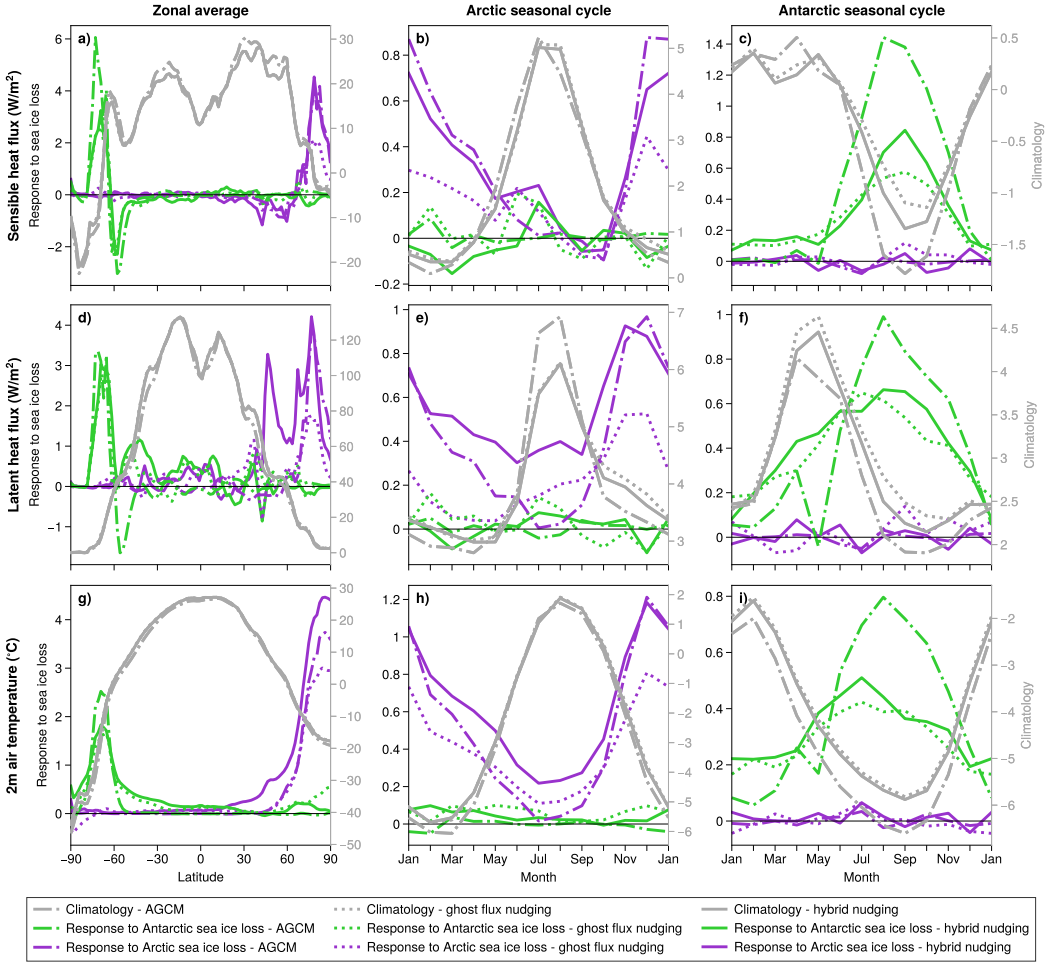

Figure 8. Zonal and annual average, and Arctic and Antarctic seasonal cycle of the turbulent heat fluxes (positive upward) and 2m air temperature climalotogies and responses to Arctic sea ice loss in the AGCM simulations and in the the fully coupled simulations with both nudging methods. a) Annual mean sensible heat flux climatology (grey), change due to Arctic sea ice loss (magenta) and change due to Antarctic sea ice loss (green). b) As in a) but for the seasonal cycle of the Arctic averaged (60°N to 90°N) sensible heat flux. c) As in b) but for the Antarctic average (60°S to 90°S) d-f) As in a-c) but for the latent heat flux response. g-i) As in a-c) but for the 2m air temperature response.

heat flux of about 3 W/m^2 around 70°S and a decrease of 1.5 W/m^2 on the equatorward flank of the 60°S latitude line. Most of the difference between the two methods in response to Antarctic sea ice loss is seen in the Antarctic seasonal cycle in Figure 8c. In fact, the largest difference occurs during the austral spring, when the hybrid nudging method leads to a larger increase in sensible heat flux (30% stronger) than the ghost-flux method, likely due to differences in sea ice cover. The AGCM response in this case shows an increase in sensible heat flux over the Antarctic that is about twice as strong as the coupled model responses. This could explain the stronger warming signal showed in Figure 7a and visible in Figure 8g (green lines).

A similar story can be told about the turbulent latent heat flux (Figures 8d-f). With both methods, a net upward latent heat flux release takes place at high latitudes in response to Arctic and Antarctic sea ice loss. However, the hybrid nudging method increases the response to Arctic sea ice loss by a factor of 2 to 3 whist both methods show a very similar response to Antarctic sea ice loss. Akin to the sensible heat flux response, the latent heat flux response to Arctic sea ice loss weakens the Arctic seasonal cycle (Figure 8e). The weakening with the hybrid nudging method is stronger than with the ghost-flux method. Once again, this is mostly due to the larger change in sea ice as the model better captures the sea ice targets with the hybrid nudging method. In the case of the latent heat flux, the AGCM response to Arctic sea ice loss matches the ghost-flux nudging response in the mid-latitudes before increasing and getting to the levels of the hybrid nudging method at high latitudes. On the other hand, both methods show very similar Antarctic seasonal responses to Antarctic sea ice loss (Figure 8f). Indeed, both methods lead to a net increase in upward latent heat flux in the Antarctic, a response that acts to weaken the abrupt seasonal decline in latent heat flux control climatology during the boreal autumn into the boreal winter.

Finally, the 2m air temperature response (Figures 8g-i) shows a similar pattern to the latent heat flux. The zonal mean near surface warming is similar for both methods in response to Antarctic sea ice loss, but the hybrid nudging methods leads to a stronger Arctic warming signal by about 1.5 °C at high latitudes in response to Arctic sea ice loss (Figure 8g). More warming arises from a larger amount of sea ice extent loss with the hybrid nudging method. The Arctic response to Arctic sea ice loss with both methods also acts to weaken the seasonal cycle in the the Arctic, although this effect is stronger

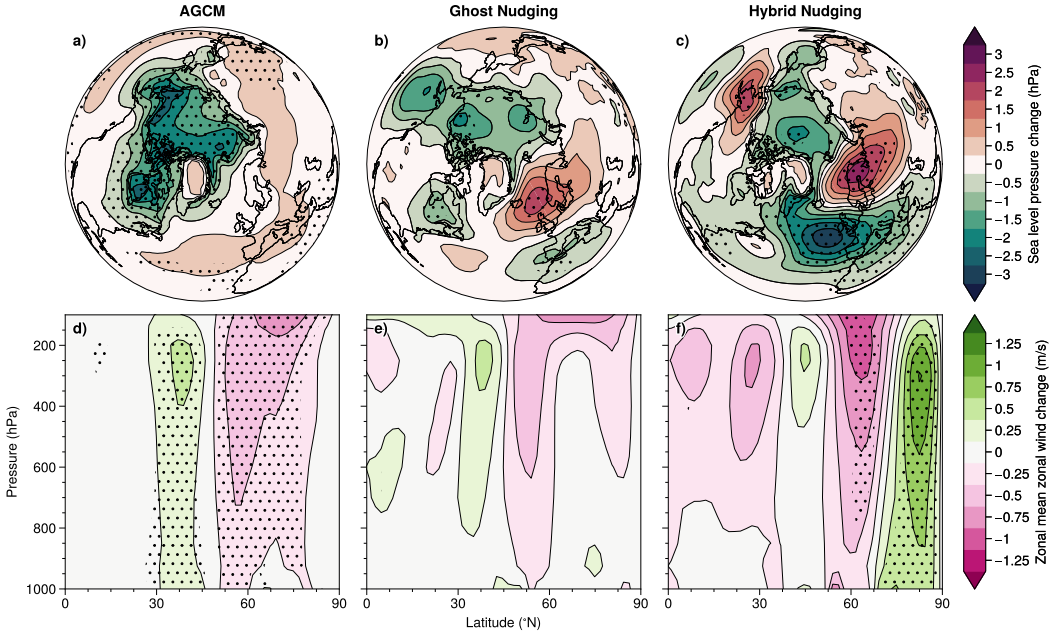

Figure 9. DJF sea level pressure and zonal mean zonal wind change with different sea ice constraining methods. a) Sea level pressure pdSST-futArcSICSIT and pdSST-pdSICSIT (prescribed SST, SIC and SIT). b) As in a) but between the pa-futArcSIC-ext-ghost and pa-pdSIC-ext-ghost experiments (ghost-flux nudging). c) As in a) but between the pa-futArcSIC-ext-hyb and pa-pdSIC-ext-hyb experiments (hybrid nudging). d)-f) As in a)-c) but for the DJF zonal mean zonal wind response. The statistical significance to a 95% confidence level with a Student t-test is indicated by the stippling.

with the hybrid nudging. Over the southern polar region (Figure 8i), the two methods show very little difference.

In addition to the surface turbulent heat fluxes and temperature responses, we compare the winter time circulation response that the different methods generate. The sea level pressure (SLP) response to Arctic sea ice loss with the AGCM setup (Figure 9a) differs significantly from the two coupled model responses (Figures 9b-c). The AGCM model leads to a SLP reduction all over the Arctic ocean with maxima that generally coincide with the temperature response in Figure 6a. The coupled model response with both nudging methods lead to a SLP increase over Scandinavia and a SLP reduction southward of the positive anomaly, a pattern absent in the AGCM signal. The response is also stronger and generally more significant when using the hybrid nudging method.

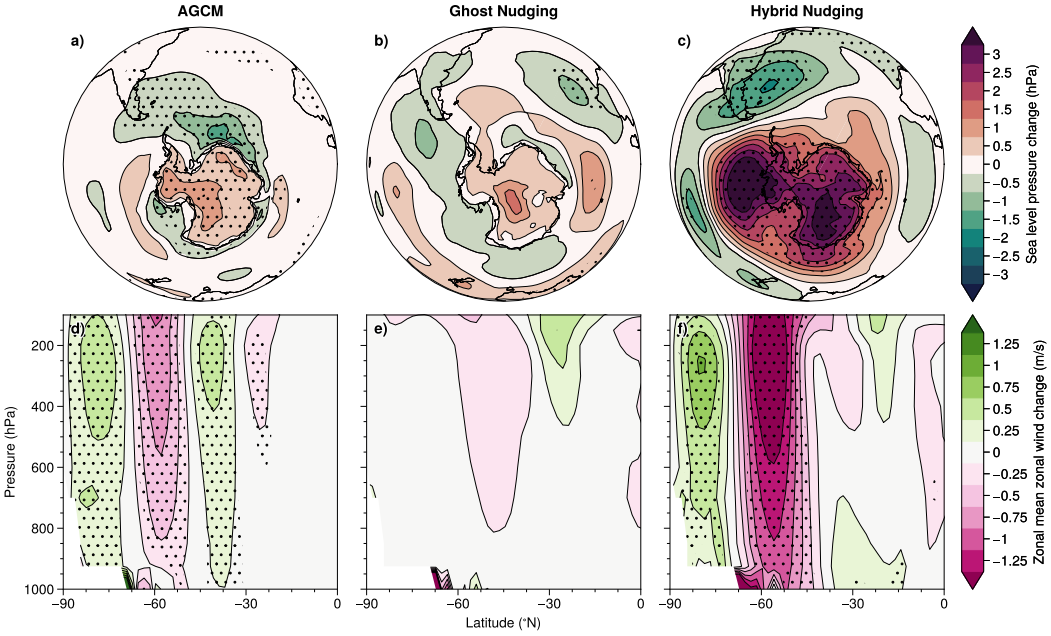

Figure 10. As in Figure 9, but for the JJA response to Antarctic sea ice loss in the Southern Hemisphere.

The zonal mean zonal wind responses also show some differences in response to Arctic sea ice loss (Figures 9d-f). In all setups, the zonal winds weaken on the poleward flank of the jet, however, the response is not significant for the ghost-flux nudging. In addition to this weakening around 60°N, the AGCM and the hybrid nudging simulations show an increase in the zonal mean zonal wind, but do not agree on the location of this signal. The AGCM response shows a significant equatorward shift of the mid-latitude jet, but the hybrid nudging experiment displays a westerly response at high latitudes. This response in the hybrid setup can be associated through thermal wind balance with the warming plume located around 70 °N in Figure 6f. Also, the westerly response at high latitudes can be seen in other AGCMs in response to similar forcings (M. M. Smith et al., 2022, Figure 2).

The austral winter circulation response to Antarctic sea ice loss also shows marked differences between the different setups (Figure 10). The AGCM SLP response (Figure 10a) shows an increase in SLP over land in Antarctica and the response shifts to a decrease over the Southern Ocean, mainly between South America and Australia. In comparison, the response obtained with the coupled model using the ghost-flux nudging shows close to no significant signal (Figure 10b). The response is noisy and is only significant

on the southwestern coast of Australia, where SLP weakens. However, the most striking difference is with the hybrid nudging response, where there is a strong positive SLP response at higher latitudes and weaker, but still significant, reductions in the midlatitudes, mostly over the southern part of South America.

The zonal mean zonal wind response to Antarctic sea ice loss is similar to the response to Arctic sea ice loss (Figures 10d-f). Again, the ghost-flux nudging experiment does not show a significant tropospheric signal, and the AGCM and hybrid nudging setups show a weakening of the poleward flank of the midlatitude jet. Here again, the AGCM shows an equatorward shift of the jet while the coupled model with hybrid sea ice nudging only shows a weakening of the easterlies at high latitudes. This time though, the AGCM response also shows this weakening at high latitudes.

3.3 Effect of remote and external forcing on the nudging

Finally, to more broadly survey characteristics of the hybrid nudging technique, we take a look at Arctic sea ice when we nudge Antarctic sea ice to the pa-futAntSIC-ext targets and when we instantaneously double the CO_2 concentrations while attempting to keep sea ice fixed to Y2000 levels. We again analyze the final 40 years of each coupled simulation.

In Figures 11a (11e) and 11b (11f), the simulated annual mean SIC (SIT) and annual mean SIC difference (SIT difference) in pa-futArcSIC-ext are shown. Both panels are there for reference and are very close to their respective targets shown in Figures 4a (4g) and 4d (4h). When Antarctic sea ice is nudged to a future state in pa-futAntSIC-ext, Arctic SIC and SIT show close to no changes (Figures 11b and 11g), as intended. Indeed, in comparison to the sea ice states in Figures 11a and 11e, SIC in pa-futAntSIC-ext-hyb has RMSE and mean bias of less than 1% and SIT has a RMSE and mean bias of less than 1 cm. Finally, when doubling the CO_2 whilst nudging sea ice in both polar regions to the pa-pdSIC-ext targets, a small amount of SIC is lost (RMSE of 1.3% and mean bias of -0.6%, Figure 11d), but no significant changes to SIT occur (RMSE of 1.6 cm and mean bias of -0.8 cm, Figure 11h). Overall, the hybrid nudging approach allows for good control over SIC and SIT even in the presence of external forcings.

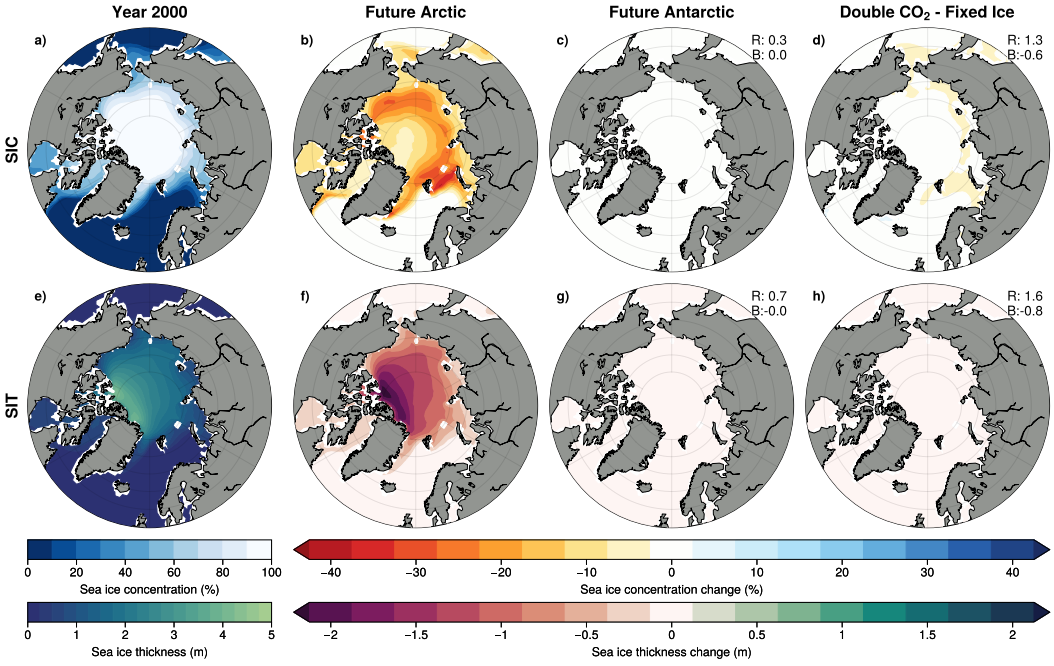

Figure 11. Annual mean Arctic SIC and SIT in the PAMIP simulations with the hybrid nudging method. a) Arctic SIC in the pa-pdSIC-ext experiment. b) Simulated Arctic SIC change between pa-futArcSIC-ext and pa-pdSIC-ext. c) As in b) but between pa-futAntSIC-ext and pa-pdSIC-ext. d) As in b) but between pa-pdSIC-2XCO2-ext and pa-pdSIC-ext. e)-h) As in a)-d) but for SIT. In the last two columns, the RMSE and mean bias are indicated as in Figures 4 and 5, treating the target here as Y2000 SIC and SIT (first column).

4 Concluding remarks

We have developed a hybrid nudging technique that combines the ghost-flux (McCusker et al., 2017; Sun et al., 2020) and direct nudging methods (D. M. Smith et al., 2017). This novel, but still relatively simple, approach allows for better control over the partitioning between SIC and SIT, but keeps the total water conservation benefit from the ghost-flux nudging method. We tested the technique using the PAMIP extended coupled simulations targets that specify the control sea ice state and projected sea ice loss in the Arctic and Antarctic separately. The hybrid nudging reduces significantly the biases over both polar regions, although the agreement with the Arctic sea ice targets remains better than for the Antarctic targets.

For the development of the nudging algorithm, we used both the fully coupled version of CESM1 with SC-WACCM4 and the sea ice component of CESM1, CICE4, driven by a data atmosphere and data ocean. Our results show that CICE4 in a stand-alone setup is a useful tool to quickly and inexpensively test sea ice constraining methods. While the full effect of the nudging method is not captured in the stand-alone setup, the results translate well qualitatively to the fully coupled model. We also note that the hybrid nudging method has only been implemented in one model (CESM1 with CICE4) and the results might vary depending on the model used. We are making the code modifications used here available to apply to other models.

Overall, the hybrid nudging method increases thin-ice melt and brings SIC much closer to target specifications. For PAMIP, this leads to greater air-sea turbulent heat exchange and warming relative to the ghost-flux nudging method. In the Arctic, this makes coupled responses more comparable to AGCM responses. The question of why the Antarctic AGCM warming is greater than the coupled warming remains to be investigated.

Our finding that the ghost-flux method does not well reproduce the PAMIP target SIC and is characterized by attenuated Arctic warming was unexpected, since the ghost-flux method has previously been shown to lead to considerable sea ice loss and strong Arctic warming in a similar model, consisting of the atmospheric component CAM4 instead of SC-WACCM4 used here (Sun et al., 2020). In the case of Sun et al. (2020), however, the target sea ice forcing is stronger (RCP8.5 forcing at the end of the twenty-first century), and we are indeed able to largely produce similar results to theirs, in our model setup with SC-WACCM4, when using their forcing (not shown). This suggests that the

inability of the ghost-flux method to capture the partitioning of between SIC and SIT is due to the weaker forcings of PAMIP, pointing to a potential source of nonlinearity and inconsistency between different sea-ice perturbation methods.

The hybrid nudging method also allows for good control over sea ice while other external or remote forcings, such as CO_2 forcing or Antarctic sea ice melt, are applied to models, meaning that this method can be very useful to isolate the impact of sea ice loss alone, as well as the effect of all other forcings without sea ice loss. We recommend this hybrid sea ice nudging method for sea ice loss coupled simulations when the effect of sea ice needs to be isolated, in particular for sea ice loss simulations with weak forcings such as the Group 6 PAMIP experiments. We argue that this method is a suitable tool for more fully addressing the issue of whether these methods generally lead to spurious polar amplification under ice loss (England et al., 2021).

Acknowledgments

The authors would like to acknowledge funding from the Ontario Graduate Scholarship and from the U.S. Department of Energy Grant DE-SC0019407. The code and instructions about modifications is available on this GitHub repository: `https://github.com/AlexAudette/hybrid-nudging`. The data used for this study is available on this dataverse page: `https://doi.org/10.5683/SP3/MRPMTM`.

References

Audette, A., Fajber, R. A., Kushner, P. J., Wu, Y., Peings, Y., Magnusdottir, G., ... Sun, L. (2021). Opposite responses of the dry and moist eddy heat transport into the arctic in the pamip experiments. *Geophysical Research Letters*, *48*(9), e2020GL089990.

Blackport, R., & Kushner, P. J. (2016). The transient and equilibrium climate response to rapid summertime sea ice loss in CCSM4. *Journal of Climate*, *29*(2), 401–417.

Blackport, R., Screen, J. A., van der Wiel, K., & Bintanja, R. (2019). Minimal influence of reduced Arctic sea ice on coincident cold winters in mid-latitudes. *Nature Climate Change*, *9*(9), 697–704. (Number: 9 Publisher: Nature Publishing Group) doi: 10.1038/s41558-019-0551-4

Carrasco, J. F., Bozkurt, D., & Cordero, R. R. (2021). A review of the observed air temperature in the Antarctic Peninsula. Did the warming trend come back after the early 21st hiatus? *Polar Science*, *28*, 100653. doi: 10.1016/j.polar.2021.100653

Cohen, J., Screen, J. A., Furtado, J. C., Barlow, M., Whittleston, D., Coumou, D., ... Jones, J. (2014). Recent Arctic amplification and extreme mid-latitude weather. *Nature Geoscience*, *7*(9), 627–637. (Number: 9 Publisher: Nature Publishing Group) doi: 10.1038/ngeo2234

Comiso, J. C., Gersten, R. A., Stock, L. V., Turner, J., Perez, G. J., & Cho, K. (2017). Positive trend in the Antarctic sea ice cover and associated changes in surface temperature. *Journal of Climate*, *30*(6), 2251–2267. (Publisher: American Meteorological Society Section: Journal of Climate) doi: 10.1175/JCLI-D-16-0408.1

Dai, A., Luo, D., Song, M., & Liu, J. (2019). Arctic amplification is caused by sea-ice loss under increasing CO2. *Nature Communications*, *10*(1), 121. (Number: 1 Publisher: Nature Publishing Group) doi: 10.1038/s41467-018-07954-9

Deser, C., Sun, L., Tomas, R. A., & Screen, J. (2016). Does ocean coupling matter for the northern extratropical response to projected Arctic sea ice loss? *Geophysical Research Letters*, *43*(5), 2149–2157.

Deser, C., Tomas, R. A., & Sun, L. (2015). The role of ocean–atmosphere coupling in the zonal-mean Atmospheric response to Arctic sea ice loss. *Journal of Cli-*

mate, *28*(6), 2168–2186. (Publisher: American Meteorological Society Section: Journal of Climate) doi: 10.1175/JCLI-D-14-00325.1

England, M., Eisenman, I., & Wagner, T. J. (2021). Spurious climate impacts in sea ice loss simulations. In *Agu fall meeting 2021.*

Eyring, V., Bony, S., Meehl, G. A., Senior, C. A., Stevens, B., Stouffer, R. J., & Taylor, K. E. (2016). Overview of the Coupled Model Intercomparison Project Phase 6 (CMIP6) experimental design and organization. *Geoscientific Model Development*, *9*(5), 1937–1958. (Publisher: Copernicus GmbH) doi: 10.5194/gmd-9-1937-2016

Hay, S., Kushner, P. J., Blackport, R., McCusker, K. E., Oudar, T., Sun, L., ... Polvani, L. M. (2022). Separating the influences of low-latitude warming and sea-ice loss on Northern Hemisphere climate change. *Journal of Climate*, *-1*(aop), 1–59. (Publisher: American Meteorological Society Section: Journal of Climate) doi: 10.1175/JCLI-D-21-0180.1

Hunke, E. C., & Lipscomb, W. H. (2010). CICE: the Los Alamos Sea Ice Model documentation and software user's manual version 4. , 76.

Hurrell, J. W., Holland, M. M., Gent, P. R., Ghan, S., Kay, J. E., Kushner, P. J., ... others (2013). The community earth system model: a framework for collaborative research. *Bulletin of the American Meteorological Society*, *94*(9), 1339–1360.

Kluzek, E. (2012). CESM research tools: CLM4 in CESM1. 0.4 user's guide documentation. *National Centers for Atmospheric Research, Boulder*.

Labe, Z., Peings, Y., & Magnusdottir, G. (2020). Warm Arctic, cold Siberia pattern: role of full Arctic amplification versus sea ice loss alone. *Geophysical Research Letters*, *47*(17), e2020GL088583.

Marsh, D. R., Mills, M. J., Kinnison, D. E., Lamarque, J.-F., Calvo, N., & Polvani, L. M. (2013). Climate change from 1850 to 2005 simulated in CESM1 (WACCM). *Journal of climate*, *26*(19), 7372–7391.

McCusker, K. E., Kushner, P. J., Fyfe, J. C., Sigmond, M., Kharin, V. V., & Bitz, C. M. (2017). Remarkable separability of circulation response to arctic sea ice loss and greenhouse gas forcing. *Geophysical Research Letters*, *44*(15), 7955–7964.

Notz, D., & Community, S. (2020). Arctic sea ice in CMIP6. *Geophysical Research*

Letters, *47*(10), e2019GL086749. doi: 10.1029/2019GL086749

NSIDC. (2022). *Sea ice index | National Snow and Ice Data Center*. Retrieved 2022-03-01, from `https://nsidc.org/data/seaice_index/`

Overland, J. E. (2016). A difficult Arctic science issue: Midlatitude weather linkages. *Polar Science*, *10*(3), 210–216. doi: 10.1016/j.polar.2016.04.011

Peings, Y., Labe, Z. M., & Magnusdottir, G. (2021). Are 100 ensemble members enough to capture the remote atmospheric response to+ 2° c arctic sea ice loss? *Journal of Climate*, *34*(10), 3751–3769.

Pithan, F., & Mauritsen, T. (2014). Arctic amplification dominated by temperature feedbacks in contemporary climate models. *Nature geoscience*, *7*(3), 181–184.

Roach, L. A., Dörr, J., Holmes, C. R., Massonnet, F., Blockley, E. W., Notz, D., ... others (2020). Antarctic sea ice area in cmip6. *Geophysical Research Letters*, *47*(9), e2019GL086729.

Scinocca, J., Reader, M., Plummer, D., Sigmond, M., Kushner, P., Shepherd, T., & Ravishankara, A. (2009). Impact of sudden arctic sea-ice loss on stratospheric polar ozone recovery. *Geophysical Research Letters*, *36*(24).

Screen, J. A., Deser, C., Smith, D. M., Zhang, X., Blackport, R., Kushner, P. J., ... Sun, L. (2018). Consistency and discrepancy in the atmospheric response to Arctic sea-ice loss across climate models. *Nature Geoscience*, *11*(3), 155–163. (Number: 3 Publisher: Nature Publishing Group) doi: 10.1038/s41561-018-0059-y

Serreze, M. C., & Francis, J. A. (2006). The Arctic amplification debate. *Climatic Change*, *76*(3), 241–264. doi: 10.1007/s10584-005-9017-y

Simon, A., Gastineau, G., Frankignoul, C., Rousset, C., & Codron, F. (2021). Transient climate response to Arctic sea ice loss with two ice-constraining methods. *Journal of Climate*, *34*(9), 3295–3310. (Publisher: American Meteorological Society Section: Journal of Climate) doi: 10.1175/JCLI-D-20-0288.1

Smith, D. M., Dunstone, N. J., Scaife, A. A., Fiedler, E. K., Copsey, D., & Hardiman, S. C. (2017). Atmospheric response to arctic and antarctic sea ice: The importance of ocean-atmosphere coupling and the background state. *Journal of Climate*, *30*(12), 4547 - 4565. doi: 10.1175/JCLI-D-16-0564.1

Smith, D. M., Eade, R., Andrews, M., Ayres, H., Clark, A., Chripko, S., ... others (2022). Robust but weak winter atmospheric circulation response to future

arctic sea ice loss. *Nature communications*, *13*(1), 1–15.

Smith, D. M., Screen, J. A., Deser, C., Cohen, J., Fyfe, J. C., García-Serrano, J., ... others (2019). The Polar Amplification Model Intercomparison Project (PAMIP) contribution to CMIP6: investigating the causes and consequences of polar amplification. *Geoscientific Model Development*, *12*(3), 1139–1164.

Smith, K. L., Neely, R., Marsh, D., & Polvani, L. M. (2014). The specified chemistry whole atmosphere community climate model (sc-waccm). *Journal of Advances in Modeling Earth Systems*, *6*(3), 883–901.

Smith, M. M., Holland, M., & Light, B. (2022). Arctic sea ice sensitivity to lateral melting representation in a coupled climate model. *The Cryosphere*, *16*(2), 419–434. (Publisher: Copernicus GmbH) doi: 10.5194/tc-16-419-2022

Smith, R., Jones, P., Briegleb, B., Bryan, F., Danabasoglu, G., Dennis, J., ... others (2010). The Parallel Ocean Program (POP) reference manual ocean component of the Community Climate System Model (CCSM) and Community Earth System Model (CESM). *LAUR-01853*, *141*, 1–140.

Sun, L., Alexander, M., & Deser, C. (2018). Evolution of the global coupled climate response to arctic sea ice loss during 1990–2090 and its contribution to climate change. *Journal of Climate*, *31*(19), 7823–7843.

Sun, L., Deser, C., Tomas, R. A., & Alexander, M. (2020). Global coupled climate response to polar sea ice loss: Evaluating the effectiveness of different ice-constraining approaches. *Geophysical Research Letters*, *47*(3), e2019GL085788. doi: 10.1029/2019GL085788